Control of electrical alternans in simulations of paced myocardium using extended time-delay autosynchronization

Carolyn M. Berger,[1,3] John W. Cain,[4] Joshua E. S. Socolar,[1,3] and Daniel J. Gauthier[1,2,3]
[1]*Department of Physics, Duke University, Durham, North Carolina 27708, USA*
[2]*Department of Biomedical Engineering, Duke University, Durham, North Carolina 27708, USA*
[3]*Center for Nonlinear and Complex Systems, Duke University, Durham, North Carolina 27708, USA*
[4]*Department of Mathematics and Center for the Study of Biological Complexity, Virginia Commonwealth University, Richmond, Virginia 23284-2014, USA*
(Received 26 February 2007; revised manuscript received 10 September 2007; published 25 October 2007)

Experimental studies have linked alternans, an abnormal beat-to-beat alternation of cardiac action potential duration, to the genesis of lethal arrhythmias such as ventricular fibrillation. Prior studies have considered various closed-loop feedback control algorithms for perturbing interstimulus intervals in such a way that alternans is suppressed. However, some experimental cases are restricted in that the controller's stimuli must preempt those of the existing waves that are propagating in the tissue, and therefore only shortening perturbations to the underlying pacing are allowed. We present results demonstrating that a technique known as extended time-delay autosynchronization (ETDAS) can effectively control alternans locally while operating within the above constraints. We show that ETDAS, which has already been used to control chaos in physical systems, has numerous advantages over previously proposed alternans control schemes.

DOI: 10.1103/PhysRevE.76.041917 PACS number(s): 87.19.Hh, 05.45.Gg

I. INTRODUCTION

Experimental studies [1–4] have linked electrical alternans, a beat-to-beat alternation of action potential duration (APD), to the genesis of lethal cardiac arrhythmias such as ventricular fibrillation. Such findings are supported by theoretical investigations [5,6] that demonstrate that large-amplitude alternans can serve as a mechanism for the breakup of spiral waves of electrical activity, leading to turbulent wave behavior reminiscent of fibrillatory patterns. It is believed that this sequence of events may be preventable by controlling alternans locally [7–9].

Alternans occurs in cardiac cells when the time interval between successive electrical stimuli, known as the basic cycle length (BCL) if pacing is periodic, reaches a critical rate. For large BCL (slow pacing), cardiac cells typically exhibit a 1:1 response in which each stimulus elicits one action potential and all APD are identical. As the BCL is decreased, the steady-state APD may become unstable [10,11] to small perturbations, resulting in alternans. Alternans can lead to higher-period rhythms, or even chaotic rhythms in which the sequence of APDs is aperiodic [12,13]. Because alternans has been linked to the onset of potentially fatal arrhythmias, it is desirable to suppress alternans in such a way that the cardiac cells resume a normal, 1:1 response.

One method for maintaining a 1:1 rhythm is to use closed-loop feedback methods that are based on real-time measurements of the cell's behavior (e.g., APD) and applying perturbations (e.g., to the BCL) designed to suppress instability. In doing so, one must be careful to distinguish between situations in which the BCL can be both lengthened and shortened and situations in which the BCL can only be shortened. As an example of the former, consider an *in vitro* preparation in which the heart's pacemaker cells, the *sino-atrial (SA) node*, have been removed. In this case, a pacing electrode has complete control of the rhythm. As an example of the latter, consider an *in vivo* experiment in which an animal's intact SA node sets the BCL. Typically, in order to take over the heart's rhythm, the controller must preempt the stimuli from the SA node, meaning that the BCL can only be shortened [7,14].

While the ultimate goal is to control whole-heart dynamics, there have been limited attempts to implement such electrical therapy [15,16]. As a step towards achieving this ultimate goal, several research groups have attempted to suppress alternans [7,17] or more complex behaviors [18] *in vitro* with preparations that have limited spatial extent. In these experiments, BCL is often determined from externally supplied electrical stimuli and small adjustments to BCL are used to maintain a 1:1 rhythm. Typically, in such experiments, it is possible to shorten or lengthen BCL, whereas for many *in vivo* preparations, it is only possible to shorten BCL.

Certain control techniques, which we refer to as *proportional* feedback methods, modify the BCL by an amount proportional to the difference between the most recently measured APD and the targeted reference state A^*. Most proportional feedback methods are similar to the Ott-Grebogi-Yorke (OGY) [19] scheme, which has been used to successfully control both periodic and aperiodic responses in physical systems. However, for the purpose of controlling alternans, OGY-type schemes have several notable disadvantages. For example, proportional feedback schemes incorporate the target APD, denoted by A^*, as a reference state, requiring knowledge of A^* prior to the initiation of control and therefore a potentially dangerous precontrol learning stage [18]. Moreover, attempts to apply proportional feedback schemes to control aperiodic cardiac rhythms have been met with limited success [18,20].

Another class of control schemes, which we refer to as *adaptive schemes*, use previous APD measurements to modify BCL, rather than referencing the unstable steady state A^*. This feature of adaptive schemes represents an ad-

vantage over the proportional feedback schemes described above since A^* is not known prior to applying control. Most adaptive schemes are similar to the one originally proposed by Pyragas [21], which has laid the foundation for many additional experimental and theoretical analyses [8,17,22–24].

Recently, Jordan and Christini [25] proposed an adaptive control scheme for the experimental control of cardiac alternans. Their scheme, known as adaptive diastolic interval control (ADIC), has several noteworthy features. First, as an adaptive scheme, ADIC does not require the use of A^* as a reference state. Moreover, as discussed by Qu [26], ADIC requires no precontrol learning phase and can be applied in a variety of dynamical regimes, both periodic and aperiodic. Finally, under certain restrictions, ADIC successfully controls alternans and chaotic rhythms while only allowing shortening of the underlying (unperturbed) BCL.

The primary purpose of this paper is to demonstrate that an adaptive control scheme known as extended time-delay autosynchronization (ETDAS) [27] exhibits great potential as a method for controlling alternans. Relative to ADIC, the ETDAS method is a more viable option for experimental control of alternans for many reasons. Notably, by writing the ADIC scheme in an apparently different but equivalent way, one finds that the ADIC scheme is actually a special case of ETDAS and the important advantages of ADIC are shared by all ETDAS schemes. ETDAS has several noteworthy features, such as (i) the control domain (i.e., the set of all possible parameter choices for which control successfully suppresses alternans) is large; (ii) various special cases of ETDAS have been used to control AV-nodal conduction time alternans in humans *in vivo* [14] as well as APD alternans in canines [7], frogs [17], and rabbits [28] *in vitro*; (iii) ETDAS is amenable to experimental setup and has already been used for chaos control in physical systems [24,29]; (iv) it is possible to restrict the ETDAS parameters to achieve control while allowing only shortening of BCL; (v) the additional freedom gained by using ETDAS as opposed to restrictive cases such as ADIC allows the experimenter to choose parameters in such a way that sensitivity to background noise is reduced; and (vi) because ETDAS has been studied for over a decade, one may exploit prior mathematical analyses [23,24] as a guide for choosing system parameters that lead to successful control of alternans.

We believe that ETDAS is an important addition to the toolkit of control schemes currently used in the electrophysiology community. To our knowledge, no one has attempted ETDAS control experimentally as a means of suppressing abnormal cardiac rhythms. This represents an exciting opportunity, given the above-mentioned list of advantages of the ETDAS method. We expect that our discussion of ETDAS will aid in future clinical studies of control by providing a detailed explanation of how to choose controller parameters.

The remainder of this paper is organized as follows. Section II contains an overview of APD restitution and mapping models, which serve as the basis for illustrating the implementation of the ETDAS method. In Sec. III, we discuss the ETDAS control method [27] as applied in the present context of suppressing alternans. The method involves two parameters: a feedback gain parameter, which represents the strength of control, and a "history" parameter, which governs the influence of past APD values upon the control perturbations. The ADIC scheme [25], a special case of ETDAS in which the two parameters must be equal, is also discussed as it serves as a useful test case throughout our study. In Sec. IV we use linear stability analysis to compute the control domain for the ETDAS method, allowing us to characterize the set of parameter choices for which control successfully suppresses alternans if lengthening the BCL is allowed. Moreover, we derive an additional necessary condition that must be satisfied if lengthening the BCL is not allowed. In doing so, we correct an error in [25] (p. 1179, line 4) in which the authors assert that methods such as ADIC, by their very construction, only allow shortening perturbations of the BCL. Because the formulation of our criteria for successful control with only shortening perturbations depends upon how control is initiated, in Sec. IV C we carefully describe how to turn on the controller. Section V and Appendix A concern the issue of minimizing sensitivity to background noise, an important consideration when attempting experimental control of alternans. We argue that, by varying the history parameter, one may reduce sensitivity to background noise while obeying the criteria for successful control. Finally, in Sec. VI we discuss the potential clinical usefulness of ETDAS as well as its limitations.

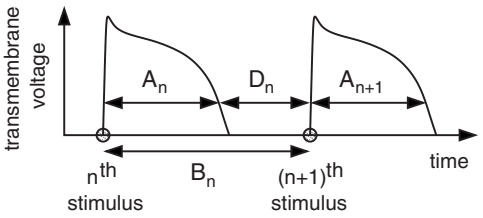

FIG. 1. Transmembrane potential for a periodically paced cardiac cell illustrating the definitions of APD and DI.

II. RESTITUTION AND MAPPING MODELS

Repeated stimulation, or *pacing*, of a cardiac cell typically elicits a train of action potentials as illustrated in Fig. 1. APD is measured with respect to a threshold voltage as shown in the figure, and the recovery time between successive action potentials is known as the diastolic interval (DI). We will denote the APD following the nth stimulus by A_n and the subsequent DI by D_n. The nth interstimulus interval will be denoted by $B_n=A_n+D_n$ and, in the special case of periodic pacing, we will write $B_n=B^*$ and refer to B^* as the BCL. In the following sections, we will assume that a controller is used to perturb the underlying BCL; i.e., $B_n=B^*+\epsilon_n$, where ϵ_n represents a perturbation.

It is well known that APD depends upon the preceding DI value, a feature of cardiac tissue known as electrical *restitution*. Shorter DI values generally result in shorter APD values. Nolasco and Dahlen [11] were among the first to model APD restitution mathematically, using a one-dimensional mapping of the form

$$A_{n+1}=f(D_n)=f(B_n-A_n). \tag{1}$$

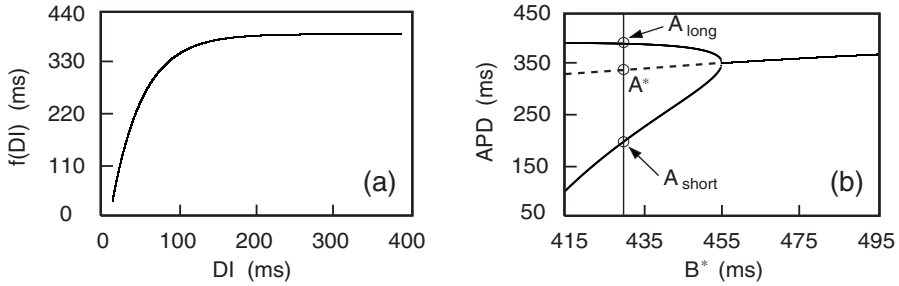

FIG. 2. (a) Graph of the restitution curve given by Eq. (2). (b) The bifurcation to alternans generated by iteration of Eq. (2) for various values of B^*. The cell exhibits 1:1 behavior for $B^*>455$ ms and alternans for shorter B^*. The dashed curve corresponds to the unstable values of APD that will be targeted during control. For $B^*=430$ ms (vertical line), A_{short}, A^*, and A_{long} are indicated.

The graph of f, known as a *restitution curve*, is illustrated in Fig. 2(a) for the particular function

$$A_{n+1}=f(D_n)=A_{\max}-\beta\exp(-D_n/\tau), \tag{2}$$

with $A_{\max}=392$ ms, $\beta=525$ ms, and $\tau=40$ ms. This particular restitution function, originally used [17] to fit bullfrog restitution data, will be used as a test case when numerical simulations are required.

Periodic pacing can lead to various phase-locked responses [30]. Large BCLs typically result in a 1:1 response in which there is no beat-to-beat variation in APD or DI. If the BCL is decreased, the cell may experience alternans, with APD alternating between A_{short} and A_{long}. Figure 2(b) illustrates a period-doubling bifurcation to alternans as the BCL is decreased.

Suppose that a cell exhibits alternans for a particular basic cycle length B^*. Alternans, although stable, is undesirable physiologically for reasons mentioned above. However, as illustrated in Fig. 2(b), there is a unique APD, denoted by A^*, which lies between A_{short} and A_{long} and corresponds to an unstable fixed point of the mapping (1). That is, $A^*=f(B^*-A^*)$. The goal of ETDAS closed-loop feedback is to apply small changes to B^* in such a way that the cell is forced to maintain a normal 1:1 response so that the sequence of APD values tends to the target value A^*.

We remark that assuming such a simple restitution relationship is done primarily for illustrative purposes, whereas it is known that cardiac cells exhibit *memory* with respect to the pacing history [31–33]. That is, A_{n+1} depends not only upon D_n, but also on previous data such as A_n and D_{n-1}. Preliminary numerical studies indicate that the control method described below is applicable even if more complicated mapping models with memory are used, although the criteria for successful control are not as simple to state.

III. ETDAS METHOD

In order to control alternans, we perturb the underlying basic cycle length B^* in each beat. Letting $B_n=B^*+\epsilon_n$, the mapping (1) becomes

$$A_{n+1}=f(B^*+\epsilon_n-A_n). \tag{3}$$

The ETDAS method [27] chooses the perturbations according to the rule

$$\epsilon_{n+1}=\gamma[A_{n+1}-A_n]+R\epsilon_n, \tag{4}$$

where R and γ are parameters. The *feedback gain* parameter γ provides a measure of the strength of the control, with $\gamma=0$ corresponding to no control. The non-negative parameter R measures the weight or influence of past values of APD upon the controller. For this reason, we refer to R as the *history parameter* for the ETDAS method. We remark that variants of the special case of ETDAS in which $R=0$ (i.e., A_{n+1} is directly influenced only by the most recent APD value A_n) have been used for experimental control of alternans both *in vivo* [14] and *in vitro* [7,17,28].

ADIC as a special case of ETDAS

In this subsection, we demonstrate that a promising, well-publicized [26] control scheme known as adaptive diastolic interval control [25] is actually a special case of the ETDAS method. The ADIC scheme adjusts DI according to the rule

$$D_{n+1}=D_n+\alpha[B^*-D_n-A_{n+1}], \tag{5}$$

where α is a constant between 0 and 1.

Note that modifying DI also modifies the interstimulus interval B_n (and vice versa) due to the relationship $A_n+D_n=B_n$ (see Fig. 1). Therefore, writing Eq. (5) in terms of perturbations of interstimulus intervals as opposed to DI leads to an apparently different (but equivalent) scheme. Indeed, since $\epsilon_n=A_n+D_n-B^*$ represents the size of the perturbation to the nth interstimulus interval, adding $A_{n+1}-B^*$ to both sides of Eq. (5) yields

$$\epsilon_{n+1}=A_{n+1}-B^*+D_n+\alpha[B^*-D_n-A_{n+1}]. \tag{6}$$

Rearranging the terms on the right-hand side of Eq. (6), we obtain

$$\epsilon_{n+1}=(1-\alpha)[A_{n+1}-A_n]+(1-\alpha)\epsilon_n. \tag{7}$$

Comparing Eqs. (4) and (7) reveals that ADIC is a special case of ETDAS with the restriction $R=\gamma=(1-\alpha)$. Observe that $\alpha=1$ corresponds to the case in which the controller is off. The ease of visualizing the control domain (defined below) for ADIC makes it a useful test case, but by eliminating the restriction $R=\gamma=(1-\alpha)$, the control domain can be significantly expanded (see Fig. 5).

IV. CONTROL DOMAIN

When assessing whether a feedback control technique is successful in suppressing alternans, one first must distinguish between experiments in which the BCL can be either lengthened or shortened and experiments in which only shortening is allowed. As an example of the former, consider an *in vitro* experiment in which the pacemaker cells have been excised. As an example of the latter, consider an *in vivo* preparation in which the pacing electrode does not overdrive the SA-nodal rhythm. In this case, the controller is constrained in that interstimulus intervals cannot be lengthened.

We define the *control domain* as the region in parameter space for which the feedback control technique succeeds if B^* can be shortened or lengthened: the APDs converge to the target steady state A^*. In the following subsections, we use linear stability analysis to determine the control domains for ETDAS and the special case of ADIC. We also derive additional conditions that the parameters must satisfy for control to succeed when we only allow for shortening of B^*.

We begin by computing the control domain for the ADIC [25,26] scheme, the special case of ETDAS in which $\gamma=R=1-\alpha$. We characterize the subregion of the control domain in which ADIC successfully suppresses alternans while allowing only shortening perturbations (i.e., $\epsilon_n<0$ for all n) of the underlying BCL.

A. Control domain for ADIC

From Eq. (7), one sees that the ADIC scheme depends upon a single control parameter α. Given an underlying B^* that promotes alternans, we wish to determine the range of α for which control successfully eliminates alternans so that $A_n \to A^*$ as $n \to \infty$. Plotting this range of α versus B^* yields the control domain for ADIC.

To determine the control domain, we linearize Eqs. (3) and (7) about the targeted steady-state response, $A_n=A^*$ and $\epsilon_n=0$ for each n. Letting $\delta A_n=A_n-A^*$, we obtain the linearized system

$$\begin{bmatrix} \delta A_{n+1} \\ \epsilon_{n+1} \end{bmatrix} = \begin{bmatrix} -s & s \\ -(1-\alpha)(s+1) & (1-\alpha)(s+1) \end{bmatrix} \begin{bmatrix} \delta A_n \\ \epsilon_n \end{bmatrix}, \tag{8}$$

where $s=f'(D^*)$ represents the slope of the restitution curve. The eigenvalues of the matrix in Eq. (8) are 0 and $(1-\alpha)(s+1)-s$. Restricting the latter eigenvalue to lie between -1 and 1 yields the requirement

$$0 < \alpha < \frac{2}{1+s}. \tag{9}$$

The control domain given by inequality (9) is not restrictive enough to ensure that only shortening perturbations of B^* are allowed. As a step towards determining conditions on α for which $\epsilon_n<0$ for all n, we avoid alternation of A_n-A^* by restricting the nonzero eigenvalue to lie between 0 and 1. This leads to the stricter inequality

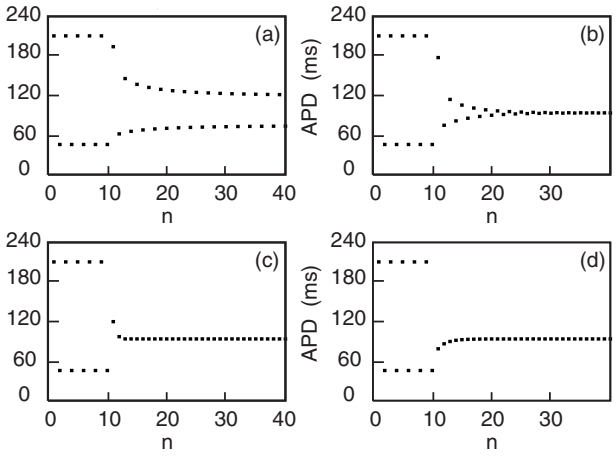

FIG. 3. Time series of APD for various choices of α. Control is initiated after the tenth beat. (a) $\alpha=0.9$, (b) $\alpha=0.8$, (c) $\alpha=0.45$, and (d) $\alpha=0.2$.

$$0 < \alpha < \frac{1}{1+s}. \tag{10}$$

For values of α satisfying this inequality, the time series of APDs should exhibit eventual monotone convergence to A^*.

Inequality (10) alone is still not enough to ensure that $\epsilon_n<0$ for all n after the controller is turned on. Motivated by Fig. 3(d) in which $\delta A_n<0$ for all n after control is initiated, one might ask whether it is possible to derive conditions on α under which *both* ϵ_n and δA_n remain negative once control is initiated. Our primary reason for imposing the additional requirement that $\delta A_n \leqslant 0$ is to facilitate the derivation of easily stated conditions on α which guarantee successful control alternans without lengthening the underlying cycle length. Indeed, one may show (see Appendix B) that if inequality (10) and the inequality

$$\alpha < \frac{A_{\text{long}} - A^*}{A_{\text{long}} - A_{\text{short}}} \tag{11}$$

are both satisfied and control is initiated in the manner described in Sec. IV C below, then $\epsilon_n<0$ and $\delta A_n<0$ for all n while the controller is on. Inequality (11) is obtained by requiring $\delta A_n<0$ in the first beat in which the controller intervenes, thereby preventing APD from "overshooting" A^*. Hereafter, we shall refer to inequality (11) as the *no-overshoot* condition for the ADIC scheme. For details, see Appendix B.

The behavior of a time series of APDs depends upon which of the inequalities (9)–(11) are satisfied. Figure 3 illustrates four sequences of APDs obtained by iterating Eqs. (3) and (7) with different choices of α. Figure 3(a) corresponds to large α (small feedback gain) that satisfies none of the inequalities. Therefore, control fails to completely suppress alternans although the amplitude is reduced. Figure 3(b) corresponds to an α that satisfies only inequality (9), yielding a sequence of APDs that alternates about A^* as the convergence takes place. Figure 3(c), in which α satisfies inequalities (9) and (10) but not inequality (11), illustrates

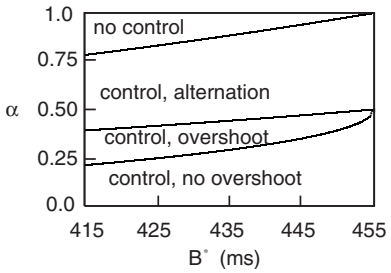

FIG. 4. The control domain for the ADIC scheme.

the overshoot issue described above. Observe that, after the controller is turned on, the first APD overshoots A^*, resulting in a sequence of APDs that *decreases* monotonically to A^*. Finally, Fig. 3(d) corresponds to an α that satisfies all of the above inequalities. After initiation of control, the APDs remain smaller than A^*, which obeys our requirements for control with only shortening perturbations ($\epsilon_n<0$). We remark that these results differ from those reported in [25], as the ADIC scheme does *not* always allow only shortening perturbations of B^*. Indeed, one must restrict α by insisting that all of the above inequalities be satisfied.

As explained in Sec. VI, we do not claim that the four responses illustrated in Fig. 3 represent all possible types of dynamical behavior. It *may* be possible for ADIC to succeed in regimes where our theoretical work suggests that control signals would have to be skipped on some beats. However, the four responses depicted in Fig. 3 provide a useful illustration of the issues one confronts when attempting to control alternans with the restriction that $\epsilon_n<0$.

Using inequalities (9)–(11), we characterize these four types of dynamical responses by dividing the control domain into three subregions as illustrated in Fig. 4. The uppermost boundary in the figure is the curve $\alpha=2/(1+s)$ and was generated by first solving for the unique DI satisfying $D^*+f(D^*)=B^*$ and then computing $s=f'(D^*)$. Above this boundary, control fails to suppress alternans (the region labeled "no control"). The region labeled "control, alternation" corresponds to values of α that satisfy (9) but not (10), resulting in alternation of A_n-A^*. The next region, labeled "control, overshoot," corresponds to values of α satisfying (10) but not (11). Finally, the lowermost region, labeled "control, no overshoot," corresponds to values of α for which all of the inequalities (9)–(11) are satisfied.

B. Control domain for ETDAS

A detailed construction of the control domain for the ETDAS method appears in Socolar and Gauthier [23]; we will apply their results in the present context of controlling alternans.

Proceeding as before, we linearize Eqs. (3) and (4) about the targeted steady-state response, $A_n=A^*$ and $\epsilon_n=0$ for each n. Letting $\delta A_n=A_n-A^*$, we obtain the linearized system

$$\begin{bmatrix} \delta A_{n+1} \\ \epsilon_{n+1} \end{bmatrix} = \begin{bmatrix} -s & s \\ -\gamma(s+1) & \gamma s+R \end{bmatrix} \begin{bmatrix} \delta A_n \\ \epsilon_n \end{bmatrix}. \tag{12}$$

To ensure that the fixed point of Eq. (12) is stable, we require that the eigenvalues have a modulus less than 1. This leads to

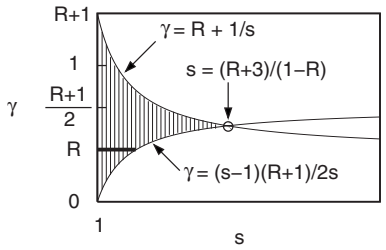

FIG. 5. The control domain for the ETDAS scheme. The value of R is assumed to be less than 1, and the two curves are given by the inequalities (13). The bold horizontal segment corresponds to the control domain for ADIC (i.e., the restriction $\gamma=R$).

the following inequalities, which constitute the control domain for ETDAS:

$$\left(\frac{R+1}{2}\right)\left(1-\frac{1}{s}\right)<\gamma<R+\frac{1}{s}, \quad R<1. \tag{13}$$

The shaded region in Fig. 5 illustrates the set of possible values of the parameter for which these inequalities are satisfied (R is assumed to be less than 1). Note that the largest possible value of s for which control can possibly succeed is given by $s=(R+3)/(1-R)$. For $s<1$, alternans is not present and there is no need to apply control.

The bold horizontal segment in Fig. 5 corresponds to the condition $R=\gamma$ imposed by the ADIC control scheme. Because this restriction effectively reduces the number of control parameters from 2 to 1, the ADIC control domain can be visualized as a "one-dimensional subset" of the ETDAS control domain as illustrated in the figure.

Although the shaded region in Fig. 5 corresponds to parameter choices for which ETDAS successfully controls alternans for positive and negative values of ϵ_n, we must restrict our choice of γ if we only allow shortening perturbations of B^* (applicable, for example, to *in vivo* preparations). Specifically, these parameters must satisfy a *no-overshoot condition* analogous to the one described in the previous subsection:

$$\gamma>\frac{A^*-A_{\text{short}}}{A_{\text{long}}-A_{\text{short}}}. \tag{14}$$

Again, we remark that this criterion presumes knowledge of A^*, the value of APD targeted by the controller. Furthermore, inequalities (11) and (14) are actually equivalent, as can be seen by recalling that $\gamma=1-\alpha$.

C. Turning on the controller

The timing of the first control perturbation is important if ETDAS is to succeed when only shortening perturbations are allowed. The aforementioned overshoot issue raises several natural questions concerning the initiation of control—for example: (i) If the tissue exhibits sustained alternans, in which beat should we "flip the switch," allowing the controller to perturb BCL? (ii) Prior to initiating control, should the controller be allowed to equilibrate by measuring ϵ_n for a few iterates? That is, should we iterate Eq. (4) along with the

uncontrolled mapping (1) before the controller is turned on?

To answer the first question, suppose that the tissue exhibits alternans between A_{short} and A_{long}. In order to ensure that transitioning from the uncontrolled mapping (1) to the controlled mapping (3) does not require lengthening an interstimulus interval, the controller should be turned on following any *short* APD [25]. Indeed, since the subsequent DI would be $D_{\text{long}} > D^*$ in the absence of control, we may shorten this DI to some DI$< D^*$ by applying a preemptive stimulus. In doing so, we assure that the next APD will be less than A^* so that we may continue to apply shortening perturbations of interstimulus intervals.

Regarding the second question, we claim that, in order to minimize the possibility of overshoot, the controller should not be allowed *any* time to equilibrate by measuring ϵ before the controller intervenes. To see why, let us establish notation by assuming that $A_{n-1}=A_{\text{long}}$, $A_n=A_{\text{short}}$, and that A_n is the last APD generated before the controller's intervention. In other words, $A_n=f(B^*-A_{n-1})$ but $A_{n+1}=f(B^*+\epsilon_n-A_n)$. If we set $\epsilon_m=0$ for $m<n$, then Eq. (4) yields $\epsilon_n=\gamma(A_{\text{short}}-A_{\text{long}})$. In order to ensure that $A_{n+1}<A^*$, we must require that $D_n<D^*$. But since $D_n=D_{\text{long}}+\epsilon_n$, we obtain the inequality

$$D_{\text{long}} + \gamma(A_{\text{short}} - A_{\text{long}}) < D^*. \tag{15}$$

Subtracting B^* from both sides yields

$$-A_{\text{short}} + \gamma(A_{\text{short}} - A_{\text{long}}) < -A^*, \tag{16}$$

from which inequality (14) follows. Now suppose that the controller is allowed one beat to equilibrate before the controller is turned on. Setting $\epsilon_m=0$ for all $m<(n-1)$ and iterating Eqs. (1) and (4) yields $\epsilon_{n-1}=\gamma(A_{\text{long}}-A_{\text{short}})$ and $\epsilon_n=\gamma(1-R)(A_{\text{short}}-A_{\text{long}})$. Proceeding as before, we impose the restriction that $D_n<D^*$ to obtain the inequality

$$\gamma(1-R) > \frac{A^* - A_{\text{short}}}{A_{\text{long}} - A_{\text{short}}}. \tag{17}$$

Observe that, since $0 \leqslant R < 1$, inequality (17) is more difficult to satisfy than the no-overshoot criterion (14). More generally, suppose that we allow the controller k beats to equilibrate so that $\epsilon_{n-k-1}=0$ and $\epsilon_{n-k}=(-1)^k\gamma(A_{\text{short}}-A_{\text{long}})$ is the first nonzero value of ϵ. Straightforward induction leads to the inequality

$$\gamma\left[\frac{1-(-R)^{k+1}}{1+R}\right] > \frac{A^* - A_{\text{short}}}{A_{\text{long}} - A_{\text{short}}}, \tag{18}$$

which again is stricter than the no-overshoot condition (14) because $0 \leqslant R < 1$. It follows that the most advantageous way to initiate control so as to avoid the overshoot issue is to (i) turn on the controller immediately after any short APD—say, $A_n=A_{\text{short}}$—and (ii) set $\epsilon_m=0$ for all $m<n$ so that the controller is not allowed any time to equilibrate.

V. DETERMINING THE CONTROLLER'S NOISE SENSITIVITY

To apply the ETDAS technique experimentally, it is important that it succeeds in the presence of background noise.

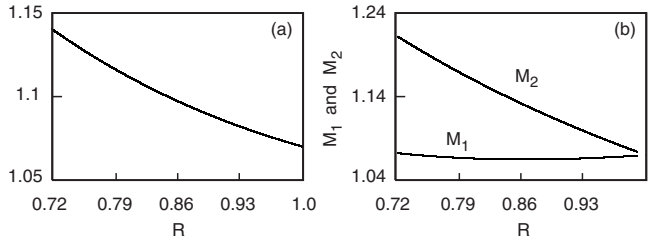

FIG. 6. (a) Decrease in amplification factor M as $R \to 1$ for $B^*=430$ ms and $\gamma=0.7325$. (b) Corresponding amplification factors for individual components of Eqs. (19) and (20). As R varies, noise amplification in ϵ decreases (M_2) whereas the noise amplification in APD remains essentially constant (M_1).

To measure sensitivity to background noise, we apply ETDAS control to a noisy version of the mapping (2). Noise is incorporated by adding a random term to the right-hand side of the mapping [25]; that is,

$$A_{n+1} = f(B^* + \epsilon_n - A_n) + \eta_n, \tag{19}$$

and hence

$$\epsilon_{n+1} = \gamma[f(B^* + \epsilon_n - A_n) - A_n] + R\epsilon_n + \gamma\eta_n, \tag{20}$$

where η_n is a normally distributed random term with mean $\mu=0$ ms and standard deviation $\sigma=10$ ms. Each η_n is independently picked from the normal distribution. We assume that the behavior of the controller is not contributing to the overall noise; it is only affected by the intrinsic noise of the system. The artificially added noise η_n is comparable to experimental limitations—for example, in guinea pig myocytes [34]. Noise sensitivity is quantified using techniques described in Egolf and Socolar [35]—specifically, we compute a noise amplification factor that represents the relative size of the standard deviation of the output sequence of controlled APD and ϵ to the standard deviation of the original input noise. For a fixed feedback gain γ, we investigate how noise sensitivity may be reduced by varying R and measuring the corresponding noise amplification factor.

By computing the noise amplification factor from Eqs. (19) and (20), our results reveal that the sensitivity to noise decreases as R increases for fixed values of s and γ. Therefore, setting $R=\gamma$ creates an unnecessary restriction on ETDAS that does not minimize the sensitivity of the control scheme to noise. To illustrate this idea, we present results from the theoretical work of Egolf and Socolar [35] and also illustrate ETDAS numerically in map (2).

Our theoretical analysis (see Appendix A) reveals that the amplification factor, which we denote by M, in general decreases with increasing R for any fixed value of γ and s. However, to achieve convergence to the unstable fixed point, R must be less than 1. For example, Fig. 6(a) was generated by choosing $\gamma=0.7325$ and $s=1.33$ and measuring M for a range of R. (Note that the time to reach the unstable fixed point A^* becomes long in the case $R \to 1$.) In general, for an unstable slope $1<s<2.09$ and $0.5<R$, $\gamma<1$, decoupling R and γ can improve the noise sensitivity up to 10%. The parameters were chosen so that a comparision could be made between the cases where $R=\gamma$ and $R \neq \gamma$ for successful con-

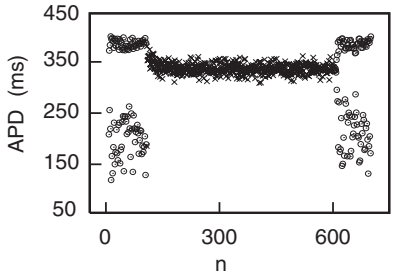

FIG. 7. Iterations of the noisy map (19) for $B^*=430$ ms. The open circles represent the uncontrolled APD values and the crosses represent the controlled APD values during ETDAS.

trol. For example, in the case when $\gamma=0.7325$ and $s=1.33$, the optimal value to minimize noise sensitivity is $R=0.99$, which equates to a 6% improvement in noise sensitivity from the case where $R=\gamma=0.7325$.

We also examine how noise affects the output sequence of controlled APD and ϵ individually by computing the components of M—i.e., M_1 and M_2 (see Appendix A for details). Figure 6(b) illustrates how M_1 and M_2 depend on R, with $\gamma=0.7325$ and $s=1.33$ fixed. Note that varying the history parameter R has a negligible impact (about 1%) on the noise amplification factor for the APD iterates (M_1). In contrast, varying R significantly impacts the noise amplification factor for the ϵ iterates (M_2), reducing noise sensitivity by up to 12% relative to the special case in which $R=\gamma$. Therefore, the primary contribution to overall noise sensitivity M arises from sensitivity of the perturbations ϵ to the controller in response to the injected noise.

Our numerical simulations confirm that M decreases with increasing R. However, the simulations also reveal that the time to reach steady state increases with increasing R and can become long in the limit as R approaches 1. Thus, we suggest choosing an optimal value of R that will minimize both the noise and the transient time to reach steady state. For the specific case where $B^*=430$ ms, we choose the pair $R=0.97$ and $\gamma=0.77$; we obtain the results shown in Fig. 7. The input level of noise in the system, $\sigma=10$ ms, is predicted to be amplified by $M_1=1.050$ for the APD iterates as determined by analysis based on Refs. [35,36] (see Appendix A), and hence the output noise for the APD iterates is theorized to be $\sigma M_1=10.50$ ms. The standard deviation computed from the last 400 noisy APD iterates of the controlled map (19) illustrated in Fig. 7 is 10.54 ms, which is in good agreement with the theoretical prediction.

VI. DISCUSSION

We have demonstrated that, within acceptable parameter ranges, the ETDAS method successfully controls alternans while allowing only shortening perturbations of the interstimulus interval. Whereas all control techniques are subject to a "no-overshoot" criterion such as (14), ETDAS succeeds for a wide range of γ, suggesting that errors in measuring (or estimating) A^* are unlikely to prevent successful control (see also "Overshoot" below). Moreover, ETDAS does not require a potentially dangerous precontrol learning phase in which numerous APD values must be recorded. In fact, the computations in Sec. IV C reveal that it is actually advantageous to allow *no* precontrol learning at all. It is especially noteworthy that ETDAS is amenable to both experimental implementation (using a recursive feedback loop with a single delay element [24,27]) and theoretical analysis via existing mathematical techniques [23]. As we have shown, it is possible to determine parameters for which (i) control succeeds and (ii) noise sensitivity is minimized.

Prior experimental and theoretical studies have reported successful control of alternans when special cases of ETDAS were used. In particular, experiments of Hall and Gauthier [17] demonstrated that the special case of ETDAS corresponding to $R=0$ can successfully control alternans in paced bullfrog tissue *in vitro*. Also, Hall *et al.* [28] applied this special case of ETDAS to control alternations in the atrioventricular (AV) nodal conduction times in rabbit heart preparations. Theoretically, the work of Jordan and Christini [25] showed that the special case of ETDAS corresponding to the restriction $R=\gamma$ (ADIC) can sometimes control alternans while allowing only shortening perturbations of the BCL. Overall, the ETDAS method is considerably more versatile in that we may simultaneously adjust the feedback gain γ and the parameter R so as to (i) successfully control alternans, (ii) minimize noise sensitivity, and (iii) allow only shortening perturbations of the BCL, which can be especially important in some *in vivo* experiments when the controller must preempt the stimuli arising from the sino-atrial node.

We now discuss several limitations of the present study.

Overshoot. One notable limitation of the ETDAS method (and all other methods mentioned in this paper) is apparent from Eq. (14): the "no-overshoot" criterion. Specifically, one cannot in principle know whether the feedback gain and history parameters will satisfy the no-overshoot condition without first knowing the value of the target steady state, A^*. Moreover, (i) in certain parameter regimes, it is possible for overshoot to occur in the second (or later) beats after the controller intervenes and (ii) in the presence of substantial background noise, inequality (14) cannot ensure that overshoot will not occur due to random fluctuations in APD. We do not attempt a technical mathematical derivation of conditions on R and γ for which the issue of overshoot is completely avoided. Instead, we performed numerical tests to confirm that there is indeed a substantial region in parameter space where the controller functions through cycle length shortening only. Figure 8 was generated by initiating control as described in Sec. IV C and recording all (R,γ) pairs for which both (i) $|\delta A_n|<10^{-9}$ after 50 beats of controller intervention and (ii) $\epsilon_n \leq 0$ for all n. Additional simulations confirmed that Fig. 8 is representative of all cycle lengths in the alternans[1] regime ($404<B^*<455$). Qualitatively, the shaded region has the same general appearance for each B^* within this range. Of course, since higher-amplitude alternans requires larger R and γ for successful control, the shaded region in Fig. 8 shrinks if B^* is reduced.

One possible remedy for overshoot is to allow the controller to be turned off [7,37] during beats which would re-

[1]Cycle lengths shorter than 404 ms generate negative APD values, and alternans is not present for cycle lengths larger than 455 ms.

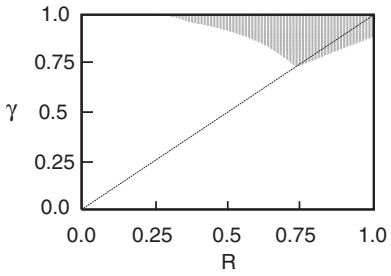

FIG. 8. Shaded region: region of parameter space for which Eqs. (3) and (4) guarantee only shortening of the underlying cycle length $B^*=430$ ms. The line $\gamma=R$, corresponding to the case of ADIC, is included for reference.

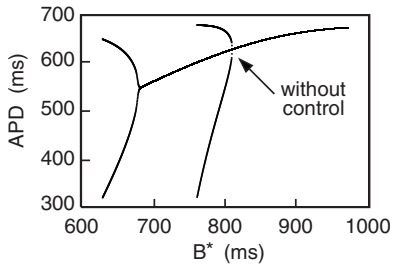

FIG. 9. Overlay of two bifurcation diagrams obtained by iteration of Eqs. (21) and (22) without control ($R=\gamma=0$) and with ETDAS control ($R=0.3$, $\gamma=0.4$).

quire lengthening the underlying BCL (i.e., beats in which $\epsilon_n>0$). Although control of alternans is achieved more slowly when the controller can be turned off and on, doing so actually *enlarges* the domain of control [37,38].

Memory. A second minor limitation of the present study concerns the use of one-dimensional mappings to model APD restitution. Whereas such mappings can give a reasonable approximation of the dynamics, cardiac tissue is known to exhibit *memory*—that is, A_{n+1} depends not only upon D_n, but also upon earlier APD and DI [31–33]. Fortunately, the ETDAS method can be applied even if a more sophisticated mapping model with memory is used. However, the resulting system of equations analogous to Eqs. (3) and (4) is higher dimensional, making it more difficult to visualize the domain of control.

To confirm the effectiveness of ETDAS in the presence of short-term memory, we performed numerical simulations of the system,

$$A_{n+1}=c_1(1-\mu_n)[1-c_2e^{-(B_n-A_n)/\tau_1}], \tag{21}$$

$$\mu_{n+1}=[1+(\mu_n-1)e^{-A_n/\tau_2}]e^{-(B_n-A_n)/\tau_2}, \tag{22}$$

where μ represents a *memory variable* [12] and, as before, $B_n=B^*+\epsilon_n$ with ϵ_n chosen according to the ETDAS method (4). For illustrative purposes, we adopt the parameter values appearing in [30]—namely, $c_1=1359$ ms, $c_2=2.64$, $\tau_1=51$ ms, and $\tau_2=1080$ ms (the results were similar for other parameter choices within the physiological regime). In the absence of control ($R=\gamma=0$), the system (21) and (22) experiences a period-doubling bifurcation at $B^*\approx 810$ ms, whereas moderate control ($R=0.3$, $\gamma=0.4$) prevents the bifurcation from occurring until $B^*\approx 680$ ms (see Fig. 9). As in our simulations of the memoryless mapping (2), with R and γ suitably chosen, Eqs. (21) and (22) can exhibit each type of response illustrated in Fig. 3. In particular, with R and γ chosen appropriately large, it is possible to control alternans without overshoot.

Spatially extended tissue. Experimental [7] and theoretical [8] studies suggest that the special case of ETDAS with $R=0$ is only able to control alternans locally (i.e., in the vicinity of the pacing electrode). Moreover, the same special case of ETDAS was unable to regularize the dynamics of *in vivo* atrial fibrillation in sheep [16]. Cardiac arrhythmias are complex, high-dimensional phenomena, and it is likely that multiple controllers would be needed for whole-heart control [9]. However, having the most robust controller at each spatial location will allow for fewer total controllers, and hence it is important to find the best local controller. We remark that the control methods described in this study are also used for controlling AV nodal conduction [28], which is essentially a one-dimensional conduction system. It remains to be seen whether the added versatility of the history parameter R makes ETDAS more successful clinically. These issues will be the subject of a future study.

ACKNOWLEDGMENTS

Support of the National Science Foundation under Grants Nos. DMS-9983320 and PHY-0549259 and the National Institutes of Health under Grant No. 1R01-HL-72831 is gratefully acknowledged.

APPENDIX A

To calculate the noise amplification factor M, we rewrite the linearization of Eqs. (19) and (20) in terms of $e_n\equiv\epsilon_n/\gamma$, obtaining

$$\begin{bmatrix}\delta A^{(n+1)}\\ e^{(n+1)}\end{bmatrix}=\begin{bmatrix}-s & \gamma s\\ -(s+1) & \gamma s+R\end{bmatrix}\begin{bmatrix}\delta A^{(n)}\\ e^{(n)}\end{bmatrix}+\begin{bmatrix}\eta^{(n)}\\ \eta^{(n)}\end{bmatrix}, \tag{A1}$$

where we have changed from subscripts to superscripts for convenience in the notation below. Although $\eta^{(n-1)}$ does not appear explicitly in the expression for $e^{(n+1)}$, its influence (and that of past η's) is embedded in $e^{(n)}$.

Letting $\mathbf{J}$ denote the Jacobian matrix in Eq. (A1) and $\mathbf{z}^{(n+1)}=(\delta A^{(n+1)},e^{(n+1)})$, Eq. (A1) can be written compactly as

$$\mathbf{z}^{(n+1)}=\mathbf{J}\cdot\mathbf{z}^{(n)}+\boldsymbol{\eta}^{(n)}. \tag{A2}$$

As discussed in [23,35,36], the noise amplification factor is given by $M=(1/\sigma)\lim_{N\to\infty}\langle|\mathbf{z}^{(N)}|^2/L\rangle^{(1/2)}$, where σ is the standard deviation of the input noise and L specifies the number of components of $\mathbf{z}^{(n+1)}$ (in our case, $L=2$). The expectation value is expressed as

$$\left\langle\frac{1}{L}|\mathbf{z}^{(N)}|^2\right\rangle=\frac{1}{L}\sum_{n=0}^{N}\sum_{r=0}^{N}\sum_{i=1}^{L}\sum_{j=1}^{L}(\lambda_{(i)})^n(\lambda_{(j)}^*)^r(\mathbf{e}_{(i)}\cdot\mathbf{e}_{(j)}^*)\times\langle(\mathbf{v}_{(i)}\cdot\boldsymbol{\eta}^{(N-n)})(\mathbf{v}_{(j)}^*\cdot\boldsymbol{\eta}^{(N-r)})\rangle, \tag{A3}$$

where n and r indicate time iterates and λ, $\mathbf{e}$, and $\mathbf{v}$ denote eigenvalues, eigenvectors, and inverse eigenvectors of $\mathbf{J}$, respectively. To simplify Eq. (A3), we assume temporally uncorrelated noise with zero mean and variance σ^2:

$$\langle \eta^{(n)} \eta^{(r)} \rangle = \sigma^2 \delta_{nr}. \tag{A4}$$

It follows that

$$\langle (\mathbf{v}_{(i)} \cdot \boldsymbol{\eta}^{(N-n)})(\mathbf{v}^*_{(j)} \cdot \boldsymbol{\eta}^{(N-r)}) \rangle = \sigma^2 \sum_{l=1}^{L} \sum_{k=1}^{L} v_{il} v^*_{jk} \tag{A5}$$

in the limit that $N \to \infty$. Substituting Eq. (A5) into Eq. (A3) and letting $N \to \infty$, the final expression for the amplification factor M simplifies to

$$M = \left(\frac{1}{L} \sum_{i=1}^{L} \sum_{j=1}^{L} \frac{1}{1 - \lambda_{(i)} \lambda^*_{(j)}} (\mathbf{e}_{(i)} \cdot \mathbf{e}^*_{(j)}) \sum_{l=1}^{L} \sum_{k=1}^{L} v_{il} v^*_{jk} \right)^{1/2}. \tag{A6}$$

Whereas Eq. (A6) provides an overall measure of noise amplification, we are also interested in how noise affects each component of $\mathbf{z}$. The expression for the amplification factor for the nth component of $\mathbf{z}$ corresponds to taking the nth component of each eigenvector. For example, if we are interested in $\mathbf{z}_{(1)}$ from Eqs. (A1), then Eq. (A6) yields

$$M_1 = \left(\sum_{i=1}^{2} \sum_{j=1}^{2} \frac{1}{1 - \lambda_{(i)} \lambda^*_{(j)}} e_{(1i)} e^*_{(1j)} \sum_{l=1}^{2} \sum_{k=1}^{2} v_{il} v^*_{jk} \right)^{1/2}. \tag{A7}$$

APPENDIX B

In this appendix, we prove that if inequalities (10) and (11) are satisfied and control is initiated as described in Sec. IV C, then *both* $\delta A_n < 0$ and $\epsilon_n < 0$ for all n. To see why, let $\mathbf{J}$ denote the coefficient matrix in Eq. (8). The eigenvalues are 0 and $\lambda = \text{trace } \mathbf{J}$, and one easily checks that $\mathbf{J}^n = \lambda^{n-1} \mathbf{J}$. Inequality (10) guarantees that $\lambda > 0$. Moreover, from Sec. IV C we know that $\delta A_0 = A_{\text{short}} - A^*$ and $\epsilon_0 = (1-\alpha)(A_{\text{short}} - A_{\text{long}})$. Thus, inequality (11) implies that $(\delta A_0 - \epsilon_0) > 0$. Finally, recalling that the slope s of the restitution curve is positive, the fact that $\delta A_n < 0$ and $\epsilon_n < 0$ for $n \geq 1$ is clear from

$$\begin{bmatrix} \delta A_n \\ \epsilon_n \end{bmatrix} = \lambda^{n-1} \mathbf{J} \begin{bmatrix} \delta A_0 \\ \epsilon_0 \end{bmatrix} = \begin{bmatrix} -s\lambda^{n-1}(\delta A_0 - \epsilon_0) \\ -(\lambda + s)\lambda^{n-1}(\delta A_0 - \epsilon_0) \end{bmatrix}.$$

To see how inequality (11) arises, suppose that control is initiated as in Sec. IV C so that $A_{n-1} = A_{\text{long}}$, $A_n = A_{\text{short}}$, and $\epsilon_n = (1-\alpha)(A_{\text{short}} - A_{\text{long}})$. From Eq. (3), we see that $A_{n+1} = f(B^* + \epsilon_n - A_{\text{short}})$. In order to ensure that $\delta A_{n+1} < 0$ (equivalently $A_{n+1} < A^*$), by monotonicity of the function f, we must require that $(B^* + \epsilon_n - A_{\text{short}}) < D^*$. Using the fact that $\epsilon_n = (1-\alpha)(A_{\text{short}} - A_{\text{long}})$ and $D^* + A^* = B^*$, routine algebra reveals that this inequality implies the no-overshoot condition (11).

[1] D. R. Adam, J. M. Smith, S. Akselrod, S. Nyberg, A. O. Powell, and R. J. Cohen, J. Electrocardiol. **17**, 209 (1984).
[2] J. M. Pastore, S. D. Girouard, K. R. Laurita, F. G. Akar, and S. Rosenbaum, Circulation **99**, 1385 (1999).
[3] D. S. Rosenbaum, L. E. Jackson, J. M. Smith, H. Garan, J. N. Ruskin, and R. J. Cohen, N. Engl. J. Med. **330**, 235 (1994).
[4] J. M. Smith, E. A. Clancy, R. Valeri, J. N. Ruskin, and R. J. Cohen, Circulation **77**, 110 (1988).
[5] F. H. Fenton, E. M. Cherry, H. M. Hastings, and S. J. Evans, Chaos **12**, 852 (2002).
[6] A. Karma, Phys. Rev. Lett. **71**, 1103 (1993).
[7] D. J. Christini, M. L. Riccio, C. A. Culianu, J. J. Fox, A. Karma, and R. F. Gilmour, Jr., Phys. Rev. Lett. **96**, 104101 (2006).
[8] B. Echebarria and A. Karma, Phys. Rev. Lett. **88**, 208101 (2002).
[9] W. J. Rappel, F. Fenton, and A. Karma, Phys. Rev. Lett. **83**, 456 (1999).
[10] M. R. Guevara, G. Ward, A. Shrier, and L. Glass, in *IEEE Computers in Cardiology* (IEEE Computer Society, Silver Spring, 1984), pp. 167–170.
[11] J. B. Nolasco and R. W. Dahlen, J. Appl. Physiol. **25**, 191 (1968).
[12] D. R. Chialvo, R. F. Gilmour, Jr., and J. Jalife, Nature (London) **343**, 653 (1990).
[13] M. Watanabe, N. F. Otani, and R. F. Gilmour, Jr., Circ. Res. **76**, 915 (1995).
[14] D. J. Christini, K. M. Stein, S. M. Markowitz, S. Mittal, D. J. Slotwiner, M. A. Scheiner, S. Iwai, and B. B. Lerman, Proc. Natl. Acad. Sci. U.S.A. **98**, 5827 (2001).
[15] W. L. Ditto, M. L. Spano, V. In, J. Neff, B. Meadows, J. J. Langberg, A. Bolmann, and K. McTeague, Int. J. Bifurcation Chaos Appl. Sci. Eng. **10**, 593 (2000).
[16] D. J. Gauthier, G. M. Hall, R. A. Oliver, E. G. Dixon-Tulloch, P. D. Wolf, and S. Bahar, Chaos **12**, 952 (2002).
[17] G. M. Hall and D. J. Gauthier, Phys. Rev. Lett. **88**, 198102 (2002).
[18] A. Garfinkel, M. L. Spano, W. L. Ditto, and J. N. Weiss, Science **257**, 1230 (1992).
[19] E. Ott, C. Grebogi, and J. A. Yorke, Phys. Rev. Lett. **64**, 1196 (1990).
[20] M. Watanabe and R. F. Gilmour, Jr., J. Math. Biol. **35**, 73 (1996).
[21] K. Pyragas, Phys. Lett. A **170**, 421 (1992).
[22] K. Pyragas, Phys. Lett. A **206**, 323 (1995).
[23] J. E. S. Socolar and D. J. Gauthier, Phys. Rev. E **57**, 6589 (1998).
[24] D. W. Sukow, M. E. Bleich, D. J. Gauthier, and J. E. S. Socolar, Chaos **7**, 560 (1997).
[25] P. N. Jordan and D. J. Christini, J. Cardiovasc. Electrophysiol. **15**, 1177 (2004).
[26] Z. Qu, J. Cardiovasc. Electrophysiol. **15**, 1186 (2004).

[27] J. E. S. Socolar, D. W. Sukow, and D. J. Gauthier, Phys. Rev. E **50**, 3245 (1994).
[28] K. Hall, D. J. Christini, M. Tremblay, J. J. Collins, L. Glass, and J. Billette, Phys. Rev. Lett. **78**, 4518 (1997).
[29] A. Chang, J. C. Bienfang, G. M. Hall, J. R. Gardner, and D. J. Gauthier, Chaos **8**, 782 (1998).
[30] G. M. Hall, S. Bahar, and D. J. Gauthier, Phys. Rev. Lett. **82**, 2995 (1999).
[31] S. S. Kalb, H. M. Dobrovolny, E. G. Tolkacheva, S. F. Idriss, W. Krassowska, and D. J. Gauthier, J. Cardiovasc. Electrophysiol. **15**, 698 (2004).
[32] E. G. Tolkacheva, M. M. Romeo, and D. J. Gauthier, Physica D **194**, 385 (2004).
[33] E. G. Tolkacheva, M. M. Romeo, M. Guerraty, and D. J. Gauthier, Phys. Rev. E **69**, 031904 (2004).
[34] M. Zaniboni, A. E. Pollard, L. Yang, and K. W. Spitzer, Am. J. Physiol. Heart Circ. Physiol. **278**, H677 (2000).
[35] D. A. Egolf and J. E. S. Socolar, Phys. Rev. E **57**, 5271 (1998).
[36] I. Harrington and J. E. S. Socolar, Phys. Rev. E **69**, 056207 (2004).
[37] D. J. Gauthier and J. E. S. Socolar, Phys. Rev. Lett. **79**, 4938 (1997).
[38] K. Hall and D. J. Christini, Phys. Rev. E **63**, 046204 (2001).